Tropical Journal of Drug Research January 2026; 3 (1): 296 - 311
ISSN: 2476-8065 (Electronic)
Available online at http://www.tjdr.org
https://doi.org/10.26538/tjdr/v3i1.2

Original Research Article

Flavonoid Scaffolds as Promising Antiviral Leads Against Varicella Zoster Virus (Chickenpox): A Structure-Guided Virtual Screening Study

Favour O. Izuagba[1], Tochukwu I. Nwakile[1], Chidi E. Duru[2], Ijeoma A. Duru[1], Lynda C. Ngozi-Olehi[3], Victor U. Obilor, Chukwuebuka D. Nwadike[1]

[1]1Computational, Organic, and Natural Product Group, Department of Chemistry, Federal University of Technology, Owerri, Nigeria
2Theoretical and Computational Chemistry Research Group, Department of Chemistry, Imo State University, Owerri, Nigeria
3Department of Chemistry, Alvan Ikoku Federal University of Education, Owerri, Nigeria
*For correspondence: Email: izuagbafavour@gmail.com, +2347041430785

Sent for review: 16 November 2025 Revised accepted: 16 January 2026

Abstract

Purpose: *Varicella-Zoster* Virus (VZV) remains a significant global health concern, particularly among immunocompromised and vulnerable populations. Limitations associated with existing antiviral therapies, including adverse effects and emerging resistance, necessitate the identification of safer and more effective alternatives. This study employed a structure-guided in-silico strategy to identify flavonoid-based inhibitors targeting VZV thymidine kinase (VZV-TK).

Methods: A curated library of 264 flavonoids was subjected to hierarchical molecular docking using the Schrödinger suite, followed by binding free energy estimation via the MM-GBSA approach. Pharmacokinetic and toxicity properties were evaluated through ADMET profiling. The most promising ligand–protein complexes were further assessed using 100 ns all-atom molecular dynamics simulations to examine binding stability and conformational behavior.

Results: Several flavonoids demonstrated strong binding affinity toward VZV-TK. Neohesperidin dihydrochalcone exhibited the most favorable binding free energy, indicating high thermodynamic stability, while naringin dihydrochalcone and myricitrin showed docking scores comparable to the co-crystallized reference ligand. Molecular dynamics analyses identified myricitrin as the most dynamically stable inhibitor, characterized by low backbone RMSD, persistent hydrogen-bonding interactions, and preserved protein compactness. ADMET predictions indicated acceptable physicochemical properties and low carcinogenicity risk for the lead compounds.

Conclusion: The integrated computational analyses highlight flavonoid scaffolds, particularly myricitrin, neohesperidin dihydrochalcone, and naringin dihydrochalcone, as promising VZV-TK inhibitors. These findings provide a strong rationale for further experimental validation and support the development of plant-derived antivirals for Varicella-Zoster Virus infection.

Keywords: *Varicella-Zoster* Virus; Flavonoids; Molecular Docking; MM-GBSA; Molecular Dynamics; ADMET

Tropical Journal of Drug Research is indexed by Chemical Abstracts, Embase, Index Copernicus, EBSCO, African Index Medicus, JournalSeek, Directory of Open Access Journals
(DOAJ), African Journal Online, Bioline International, Open-J-Gate and Pharmacy Abstracts

INTRODUCTION

Varicella-zoster virus (VZV), a member of the human alphaherpesvirus family, is the etiological agent responsible for varicella, commonly referred to as chickenpox. Primary infection with VZV typically occurs during childhood in immunocompetent individuals, presenting as an acute, self-limiting disease characterized by a vesicular exanthema accompanied by mild systemic symptoms such as fever, malaise, and myalgia. However, in immunocompromised patients, pregnant women, and even otherwise healthy adults, VZV infection may progress to severe disease, often due to complications arising from bacterial superinfections, pneumonia, encephalitis, or disseminated VZV, which can result in hospitalization or mortality.[1] The global burden of varicella remains substantial, particularly in low- and middle-income countries. According to the World Health Organization (WHO), varicella accounts for an estimated 140 million cases annually worldwide, leading to approximately 4.2 million cases with severe complications requiring hospitalization, and 4200 deaths each year.[2] Epidemiological patterns of varicella differ markedly between temperate and tropical regions. In temperate climates, primary VZV infection typically occurs during early childhood; in contrast, individuals in tropical regions tend to acquire the infection later in life, increasing their risk of complications. In Nigeria, seroepidemiological data indicate that approximately 50 % of children aged 4–6 years possess detectable varicella antibodies, suggesting prior exposure to the virus. This seropositivity rises to about 70 % among adolescents aged 13–15 years,[3] highlighting a delayed pattern of varicella acquisition compared to temperate populations.

Varicella is the clinical manifestation of primary VZV infection and is among the most contagious human diseases due to its airborne transmission. Following inhalation, the virus replicates in the upper respiratory tract, particularly in the tonsils and local lymphoid tissues, before disseminating systemically through infected T-lymphocytes. After an incubation period of 10–21 days, the infection culminates in the appearance of a characteristic vesicular rash. The virus is subsequently transported by T-cells to the skin, where it infects epidermal cells and may be modulated by local interferon-α responses. Simultaneously, the virus establishes latency by retrogradely migrating to the sensory ganglia, where it remains dormant under the control of host cellular immunity.[4] In some individuals, particularly the elderly or immunocompromised, the decline in immune surveillance can lead to viral reactivation, manifesting clinically as herpes zoster.[5] Although antiviral therapies such as acyclovir, valacyclovir, and famciclovir are standard treatments for VZV, their use is limited by safety concerns. Acyclovir, a guanosine analogue, and its prodrug valacyclovir, offer moderate efficacy but are associated with adverse effects including nephrotoxicity, neurotoxicity, and gastrointestinal disturbances. Famciclovir, while better tolerated, may cause rare but serious side effects such as neutropenia and central nervous system effects.[6] These limitations underscore the necessity for safer and more effective antiviral agents with improved pharmacological profiles.

Given the limitations of current antiviral therapies, attention has increasingly shifted toward plant-derived compounds as promising alternatives. Medicinal plants such as *Azadirachta indica* (neem), *Curcuma longa* (turmeric), and *Echinacea purpurea* (purple coneflower) have demonstrated notable antiviral activity by directly inhibiting viral replication, modulating host immune responses, and reducing inflammation.[7] Phytochemicals including emodin, quercetin, myricetin, resveratrol, and silymarin have shown broad-spectrum efficacy against various human viruses in both in-vitro and in-vivo models, highlighting their potential as scaffolds for novel antiviral drug development.[8] These natural compounds may offer synergistic benefits when used alongside conventional antivirals, improving therapeutic outcomes. The relevance of such alternative therapeutics is underscored by recent outbreaks of chickenpox, such as the one reported in 2023 at the Agagbe Internally Displaced Persons (IDP) camp in Gwer Local Government Area of Benue State, Nigeria.[9] In response to such public health threats, the Nigeria Centre for Disease Control (NCDC), in collaboration with international partners including the WHO and CDC, continues to strengthen laboratory diagnostics, surveillance systems, and outbreak response frameworks.[10] Despite these efforts, the persistent burden of VZV infections in vulnerable populations accentuates the need for safer, more effective, and accessible antiviral strategies, including those derived from phytomedicine.

In light of these therapeutic challenges and the promise shown by plant-derived antivirals,this study adopted a comprehensive in-silico strategy to systematically investigate flavonoid-based compounds as potential inhibitors of VZV. The computational workflow integrated molecular docking, MM-GBSA binding free energy estimation, ADMET profiling, and subsequent

molecular dynamics (MD) simulations to enable robust identification and validation of promising lead candidates. Molecular docking was initially employed to screen a curated library of flavonoids against the viral target site, allowing assessment of binding affinities and characterization of key ligand–protein interaction patterns. The top-ranked complexes were further subjected to MM-GBSA analysis to quantify binding free energies and evaluate the thermodynamic favorability of ligand association. ADMET profiling was then conducted to examine the pharmacokinetic behavior, toxicity risks, and overall druglikeness of the shortlisted compounds, thereby ensuring selection of candidates with favorable safety and bioavailability attributes. Following ADMET filtration, all-atom MD simulations were performed on the most promising ligand–protein complexes to assess their dynamic stability, conformational behavior, and interaction persistence under physiologically relevant conditions. By integrating these methodologies, this study not only identified flavonoid compounds with strong binding affinities and favorable pharmacological characteristics but also demonstrated the utility of computational tools in accelerating early-stage antiviral drug discovery.

MATERIALS AND METHODS

Computer System Properties and Workflow

Figure 1: Computational modelling workflow

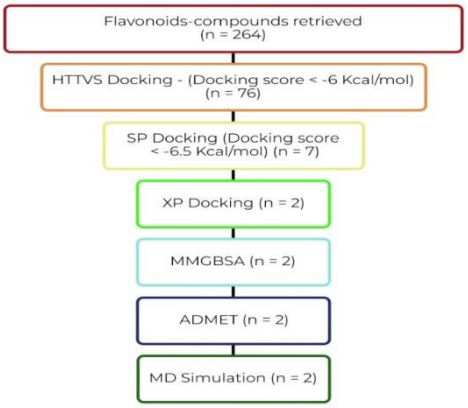

All computational analyses in this study were conducted using an integrated workflow combining the Schrödinger software suite (Maestro interface) and the KNIME analytics platform. The simulations were executed on an HP laptop workstation equipped with an Intel® Core™ i7 processor (2.6 GHz, 8 cores), 16 GB of RAM, and a 64-bit Windows 10 operating system. This computational setup provided the processing power and memory required to efficiently manage and analyze large-scale virtual screening and molecular modeling tasks. The workflow architecture, as depicted in Figure 1, ensured seamless integration of structure-based drug design tools and cheminformatics pipelines for accurate and reproducible results.

Protein Preparation and Receptor Grid Generation

The crystal structure of the varicella zoster virus in complex with the inhibitor (e)-5-(2-bromovinyl)-2'-deoxyuridine-5'-monophosphatewas retrieved from the Protein Data Bank (PDB ID: 1OSN), with a reported resolution of 3.20 Å. The protein structure was first imported into the Schrödinger Maestro workspace for preprocessing. Missing loops and side chains were reconstructed using the Prime module, followed by refinement steps that included the systematic removal of water molecules. pH optimization was carried out at pH 7.5 using PROPKA, and water molecules beyond a 5 Å radius from heteroatoms were subsequently removed. The protein structure was then energy-minimized using the OPLS3e force field to achieve a low-energy, stable conformation suitable for docking analysis. Following minimization, a receptor grid was generated using the Glide module to define the ligand-binding site. The co-crystallized ligand was retained in the binding pocket to guide the grid definition but was excluded from the grid calculation to prevent bias during ligand docking.[11] The receptor grid was generated using a van der Waals radius scaling factor of 1.0 and a partial charge cutoff of 0.25, with all other parameters (site constraints, rotatable groups, excluded volumes) set to default. The final grid was centered at coordinates x: – 83.29, y: 22.32, z: 56.56, and used as the docking reference for subsequent virtual screening experiments.

Ligand Preparation

A total of 264 flavonoid compounds were downloaded from https://www.selleckchem.com/screening/Flavonoid-Compound-Library.html and used for the virtual screening. Ligand preparation was performed using the LigPrep module in Schrödinger Maestro, ensuring structural consistency and chemical accuracy prior to docking. Preparation was conducted at pH 7.0 using the LigPrep node, and the OPLS3 force field was applied for energy minimization. Tautomer generation was disabled, and stereoisomer generation was restricted to a single isomer per compound to reduce computational redundancy. The resulting structures were saved in Maestro output format

(.mae) for compatibility with downstream docking protocols. In addition to the flavonoid library, the co-crystallized ligand, valacyclovir, and famciclovir were included as reference compounds to serve as benchmarks for comparative docking performance. These reference ligands underwent identical preparation procedures to ensure methodological consistency. Their inclusion facilitated the evaluation of binding affinities and interaction profiles of the test compounds relative to known or structurally characterized inhibitors, thereby enhancing the robustness and interpretability of the docking results.

Validation of the Molecular Docking Protocol

To ensure the reliability and predictive accuracy of the molecular docking procedure, a docking validation step was systematically carried out. This process involved the re-docking of the native co-crystallized ligand into the active site of its corresponding target protein structure, which had been preprocessed and energy-minimized to attain an optimal conformation for docking simulations. The ligand was separated from the protein complex and subsequently reintroduced into the same binding pocket using the established docking parameters and grid configuration. The docking protocol was considered valid if the re-docked pose exhibited a root mean square deviation (RMSD) of less than 2.0 Å relative to the original crystallographic orientation of the ligand, indicating that the software was capable of accurately reproducing known binding modes.

Molecular Docking Studies

Molecular docking was employed to explore the binding interactions between the prepared flavonoid compounds and the active site of the VZV, providing insights into their potential inhibitory activity and molecular recognition mechanisms. The docking studies were performed using the Glide module within the Schrödinger Maestro interface, utilizing a flexible docking protocol to accommodate ligand conformational variability. Ligands previously prepared via the LigPrep Node, along with the receptor grid generated using the Receptor Grid Generation Node, were used as inputs for the docking simulations. The docking workflow was executed in a three-tiered precision scheme to progressively refine compound selection. Initially, all ligands were screened using the High Throughput Virtual Screening (HTVS) mode to rapidly assess binding potential and eliminate low-affinity candidates. Compounds with favorable docking scores were then subjected to a second round of docking using the more accurate Standard Precision (SP) mode, allowing for enhanced assessment of binding orientations and affinities. Finally, the top performing ligands from the SP phase were redocked using the Extra Precision (XP) mode, which applies a more rigorous scoring function and deeper sampling of ligand conformations. This stepwise approach ensured the identification of high-affinity binders with optimal interaction profiles for further evaluation.

Molecular Mechanics Generalized Born Surface Area (MM-GBSA) Analysis

The Molecular Mechanics-Generalized Born Surface Area (MM-GBSA) approach is a widely adopted post-docking technique used to estimate the binding free energy (ΔG_{bind}) of ligand receptor complexes. This method decomposes the total energy contributions from various components of a molecular system, including the optimized free protein ($G_{protein}$), the free ligand (G_{ligand}), and the protein–ligand complex ($G_{complex}$). The binding free energy, which reflects the thermodynamic favorability of ligand association, is computed using equation 1.

$$\Delta G_{binding} = G_{complex} - \left(G_{protein} + G_{ligand}\right) \quad (1)$$

In this study, MM-GBSA calculations were performed using the Prime module integrated within the Maestro interface of the Schrödinger suite. The OPLS3 force field was employed in conjunction with the VSGB 2.0 implicit solvent model to accurately simulate solvation effects and conformational energetics. Additionally, Prime rotamer search algorithms were applied to refine side-chain orientations and minimize steric clashes, thereby enhancing the accuracy of energy estimations. The resulting $\Delta G_{binding}$ values provide critical insights into the thermodynamic favorability of candidate ligands, complementing docking scores and guiding lead optimization efforts.[12]

ADMET Analysis

Following the identification of flavonoid compounds through molecular docking, a comprehensive in-silico pharmacokinetic and toxicity evaluation was conducted to assess their druglikeness and suitability for further development. This evaluation included the hit compounds, valacyclovir and famciclovir, which served as reference compounds. ADMET (Absorption, Distribution, Metabolism, Excretion, and Toxicity) analysis,[13] was performed using the ADMETlab 3.0 web server, a robust and widely used computational platform that predicts key

pharmacokinetic and toxicity parameters based on molecular structure.

Molecular dynamics simulation of protein-ligand complex

All-atom molecular dynamics (MD) simulations were employed to complement the static interaction profiles obtained from molecular docking and to investigate the dynamic stability and conformational behavior of the ligand–receptor complex under physiologically relevant conditions.[14,15] The lead phytochemical compound, selected based on its superior docking affinity toward the VZV, was subjected to a 100 ns MD simulation using the Desmond module implemented in Schrödinger LLC (Schrödinger Release 2019-4). Prior to simulation, the protein–ligand complex was prepared using the Protein Preparation Wizard, which included correction of bond orders, protonation and hydrogen atom assignment, optimization of the hydrogen-bonding network, and restrained energy minimization to relieve steric clashes. The prepared complex was subsequently solvated within an orthorhombic periodic boundary box using the System Builder, employing SPC water molecules and the OPLS all-atom force field to accurately describe interatomic interactions. System electroneutrality was achieved by the addition of appropriate counterions, and an ionic strength of 0.15 M NaCl was applied to mimic physiological conditions. The MD simulation was carried out under isothermal–isobaric (NPT) ensemble conditions, maintaining the temperature at 300 K and pressure at 1 atm using the Berendsen thermostat and barostat, respectively. Following initial energy minimization and stepwise equilibration, the production run was executed for 100 ns. Trajectory frames were saved at 10 ps intervals for post-simulation analyses. The structural stability of the protein–ligand complex and the persistence of ligand binding within the active site were assessed by monitoring the root mean square deviation (RMSD) of the protein backbone atoms throughout the simulation period.

RESULT AND DISCUSSION

Validation of docking protocol

The structural superimposition of the co-crystallized ligand in its original crystallographic pose (red) and its re-docked conformation (green) within the active site of the minimized 1OSN protein structure is shown in Figure 2. This visual comparison serves as a critical step in validating the docking protocol, demonstrating the ability of the docking software to accurately reproduce the experimentally observed binding mode. The close alignment of the two ligand conformations indicates a high level of precision in the docking setup, confirming its suitability for virtual screening.

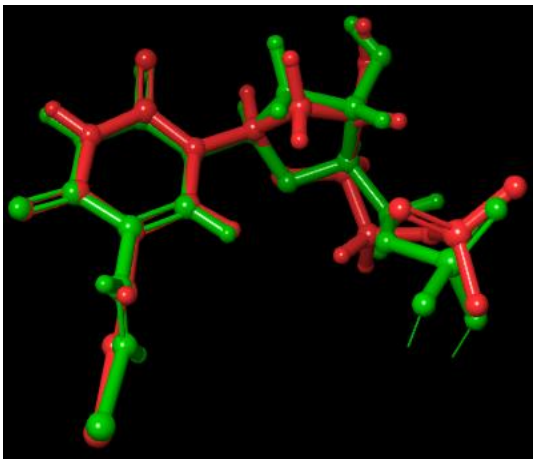

Figure 2: Superimposition of the co-crystallized ligand (Red- Original, Green- after docking) in its original position and after docking

The resulting RMSD between the docked pose and the original crystallographic pose was 0.9434 Å. This indicates a perfect superimposition, which strongly supports the reliability of the docking protocol employed in this study. In structure-based drug design, an RMSD value ≤ 2.0 Å is generally accepted as a benchmark for reliable docking performance.[16] The observed value not only meets but surpasses this threshold, confirming that the docking protocol, including the grid box dimensions, scoring function, and minimization settings, was appropriately configured and highly accurate. Such a result provides strong internal validation for the entire docking workflow. These findings justify the subsequent interpretation of docking scores for the phytochemical candidates.

Molecular docking studies

The binding energies (in kcal/mol) of the top-ranking flavonoid compounds identified through XP molecular docking against the active site of VZV thymidine kinase (VZV-TK) are given in Table 1.

Table 1: Binding energy of flavonoids from the extra precision docking analysis

Compound	Binding energy (kcal/mol)
Co-crystallized ligand	-14.461

Naringin Dihydrochalcone	-12.854
Myricitrin	-12.473
Valacyclovir (Control)	-5.695
Famciclovir (Control)	-4.768

A multi-tiered molecular docking strategy was employed in this study to identify potential flavonoid-based inhibitors of Varicella zoster virus thymidine kinase. The virtual screening workflow incorporated three progressively stringent docking protocols using the Glide module: High Throughput Virtual Screening (HTVS) for rapid initial filtering, Standard Precision (SP) for intermediate refinement, and Extra Precision (XP) for detailed assessment of ligand-receptor interactions. This hierarchical approach enabled the efficient narrowing of the compound pool, prioritizing molecules with the most favorable binding profiles for in-depth analysis. The XP docking mode, which applies a more rigorous scoring function and enhanced sampling of ligand conformations, was used to evaluate the top candidates from the previous stage. Among the evaluated compounds, the co-crystallized ligand exhibited the most favorable binding energy (−14.461 kcal/mol), serving as a reliable benchmark that validates the docking protocol and confirms the structural integrity of the binding pocket. Importantly, two flavonoid compounds, Naringin dihydrochalcone (−12.854 kcal/mol) and Myricitrin (−12.473 kcal/mol) demonstrated remarkably strong binding affinities, approaching that of the native ligand. This proximity in binding energy suggests that these flavonoids can effectively occupy and stabilize the active site, potentially mimicking or disrupting native protein–ligand interactions essential for viral function. In contrast, the standard antiviral drugs Valacyclovir (−5.695 kcal/mol) and Famciclovir (−4.768 kcal/mol) displayed substantially weaker binding energies within the same docking framework. While these nucleoside analogs are clinically effective through intracellular phosphorylation and inhibition of viral DNA polymerase, their relatively poor docking scores underscore a key mechanistic distinction: their antiviral efficacy is not primarily driven by high-affinity binding at the evaluated protein site. This disparity highlights the advantage of flavonoid scaffolds, which appear to engage the target protein more directly and robustly at the molecular level. The superior binding affinities observed for Naringin dihydrochalcone and Myricitrin can be attributed to their polyphenolic architecture, which enables extensive hydrogen bonding, π–π stacking, and hydrophobic interactions within the binding cavity. Additionally, their glycosylated moieties may contribute to enhanced spatial complementarity and interaction density, reinforcing binding stability. These structural features align with the growing recognition of flavonoids as privileged scaffolds in antiviral drug discovery. Positioned within the broader research framework, these findings reinforce the central hypothesis that structure-guided virtual screening can uncover natural-product–based antiviral candidates with binding efficiencies surpassing existing controls at the target-protein level. The pronounced binding advantage of the flavonoids over standard drugs suggests their potential utility either as standalone antiviral leads or as templates for further lead optimization through bioisosteric modification and structure–activity relationship (SAR) studies.

Protein-ligand interaction analysis

To further understand the binding mechanisms underlying the docking results, the key amino acid residues involved in ligand–protein interactions were identified and compared across all screened compounds and control drugs (Figure 3). Table 2 presents the specific residues interacting with each ligand, highlighting both conserved and unique interactions within the active site.

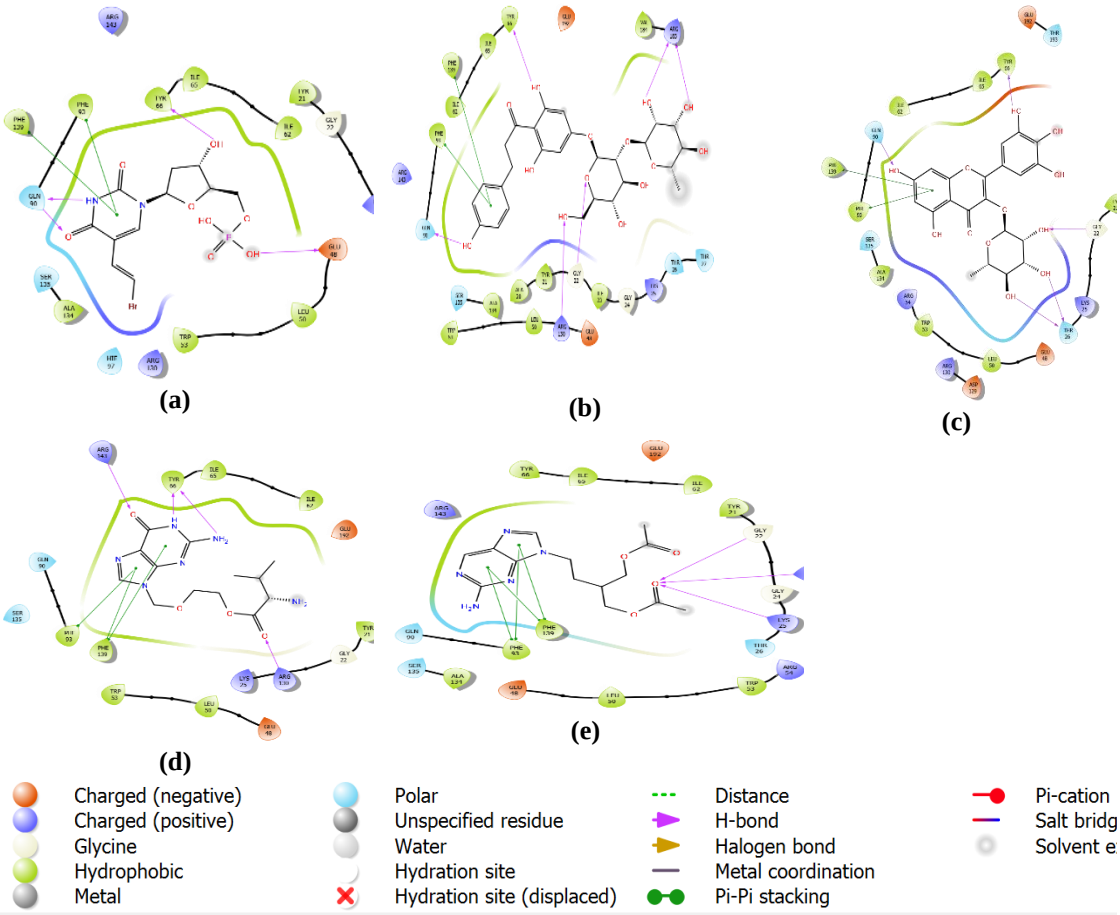

Figure 3: 2D protein-ligand interactions for (a) Co-crystallized ligand, (b) Naringin Dihydrochalcone, (c) Myricitrin, (d) Valacyclovir (Control), (e) Famciclovir (Control)

Table 2: Hydrogen bonding between ligands and VZV thymidine kinase active site residues

Ligands	Hydrogen bonding interacting amino acids	Hydrophobic interacting amino acids	Other interactions
Co-crystallized ligand	GLU 48; LYR 66; GLN 90	TYR 21; LEU 50; TRP 53; ILE 62; ILE 65; TYR 66; PHE 93; ALA 134; PHE 139	GLY 22; LYS 25; PHE 93; HIE 97; ARG 130; SER 135; PHE 139; ARG 143
Naringin Dihydrochalcone	GLY 22; TYR 66; GLN 90; ARG 130; ARG 183	ALA 20; TYR 21; ILE 23; LEU 50; TYP 53; ILE 62; ILE 65; TYR 66; PHE 93; ALA 134, PHE 139; VAL 184	GLY 24; LYS 25, THR 26; THR 27; GLU 48; SER 135; ARG 143; ARG 183; GLU 192;
Myricitrin	GLY 22; THR 26; TYR 66; GLN 90	TYR 21; LEU 50; TRP 53; ILE 62; ILE 65; TYR 66; PHE 93; ALA 134; PHE 139	LYS 25; GLU 48, ARG 54; ASP 129; ARG 130; SER 135; GLU 192; THR 193
Valacyclovir (Control)	TYR 66; ARG 130; ARG 143	TYR 21; LEU 50; TRP 53; ILE 62; ILE 65; TYR 66; PHE 93; PHE 139	GLY 22; LYS 25; GLU 48; GLN 90;PHE 93; ARG 130; SER 135; PHE 139; ARG 143; GLU 192
Famciclovir (Control)	GLY 22; LYS 25; AR 130	TYR 21; LEU 50; TRP 53; ILE 62; ILE 65; TYR 66; PHE 93, ALA 134; PHE 139	GLY 24; THR 26; GLU 48; ARG 54; PHE 90; PHE 93; SER 135; PHE 139; ARG 143; GLU 192

A detailed interaction analysis was performed to elucidate the molecular basis underlying ligand recognition and stabilization within the active site of VZV-TK. Hydrogen bonding, hydrophobic contacts, and auxiliary electrostatic interactions were systematically evaluated to rationalize the observed docking affinities and to position flavonoid scaffolds within the antiviral drug-design framework. The co-crystallized ligand establishes a well-defined interaction network characterized by hydrogen bonds with GLU48, LYS66, and GLN90, residues that are known to play a critical role in substrate recognition and catalytic efficiency of viral thymidine kinases. This ligand further engages an extensive hydrophobic pocket comprising TYR21, LEU50, TRP53, ILE62, ILE65, TYR66, PHE93, ALA134, and PHE139, thereby stabilizing its binding orientation. Additional polar and electrostatic interactions involving LYS25, ARG130, SER135, and ARG143 reinforce the ligand's residence within the active site, serving as a structural reference for evaluating candidate compounds. Notably, Naringin dihydrochalcone demonstrated a highly favorable interaction profile that closely mirrored, and in some aspects exceeded, that of the native ligand. It formed multiple hydrogen bonds with GLY22, TYR66, GLN90, ARG130, and ARG183, indicating strong anchoring at key catalytic and recognition residues. The involvement of ARG130, a residue repeatedly implicated in nucleotide binding and phosphoryl transfer, suggests a plausible inhibitory mechanism through direct competition with natural substrates. Moreover, the ligand engaged a broad hydrophobic surface encompassing ALA20, TYR21, LEU50, TRP53, ILE62, ILE65, PHE93, ALA134, and PHE139, enhancing binding stability. Supplementary interactions with GLU48, SER135, ARG143, and GLU192 further contributed to electrostatic complementarity and structural cohesion within the binding pocket. Similarly, Myricitrin exhibited a conserved hydrogen-bonding pattern involving GLY22, THR26, TYR66, and GLN90, residues that are also engaged by the co-crystallized ligand. This overlap highlighted a shared binding mode and supports the structural validity of Myricitrin as a VZV-TK inhibitor. The hydrophobic interactions formed with TYR21, LEU50, TRP53, ILE62, ILE65, PHE93, ALA134, and PHE139 indicated efficient occupation of the enzyme's hydrophobic cavity. Additional electrostatic contacts with ARG130, SER135, and GLU192 suggested enhanced ligand stabilization and may partially explain the favorable binding energies observed during docking analysis. In contrast, the control drugs Valacyclovir and Famciclovir displayed comparatively limited hydrogen-bonding networks. Valacyclovir interacted via hydrogen bonds with TYR66, ARG130, and ARG143, while Famciclovir primarily engaged GLY22, LYS25, and ARG130. Although these interactions involve functionally relevant residues, the overall interaction density and hydrogen-bond multiplicity are markedly lower than those observed for the flavonoid compounds. This finding aligns with the pharmacological mechanism of these drugs, which rely on intracellular activation rather than high-affinity binding to VZV-TK at the docking stage. Collectively, the interaction profiling revealed that flavonoid scaffolds, particularly Naringin dihydrochalcone and Myricitrin, established extensive and functionally relevant hydrogen-bonding and hydrophobic networks within the VZV active site. The conservation of key interactions with residues such as GLU48, TYR66, GLN90, and ARG130 underscored their potential to disrupt enzymatic activity effectively. These results strongly support the hypothesis that flavonoid-based compounds can serve as structurally robust and mechanistically viable antiviral leads against Varicella Zoster Virus.

MM-GBSA calculation

The $\Delta G_{binding}$ of the top-performing flavonoids, alongside the co-crystallized ligand, Valacyclovir and Famciclovir, are summarized in Table 3. These values provide a metric to identify lead compounds with not only favorable binding poses but also energetically stable interactions with the VZV-TK.

The Molecular Mechanics Generalized Born Surface Area (MM-GBSA) method is a widely accepted computational approach for estimating the binding free energy ($\Delta G_{binding}$) of protein ligand complexes, offering a critical refinement step following molecular docking.[17] It integrates molecular mechanics (MM) energies with an implicit solvation model based on the generalized Born (GB) approximation and surface area (SA)-dependent non-polar solvation contributions.[18]

Table 3: Binding free energy of top-scoring compounds and controls

Chemical Compounds	$\Delta G_{binding}$
Co-crystallized ligand	-84.23
Naringin Dihydrochalcone	-65.14
Myricitrin	-52.66
Valacyclovir (Control)	-36.41
Famciclovir (Control)	-50.57

MM-GBSA is particularly valued in structure-based drug design due to its favorable balance between computational efficiency and accuracy, outperforming conventional docking scoring functions while remaining significantly less resource-intensive than more rigorous alchemical free energy methods.[19] In this study, MM-GBSA calculations were performed using the Prime module of the Schrödinger suite to provide quantitative thermodynamic insight into the binding strength of the flavonoid hit compounds identified from the docking analysis. This approach accounts for van der Waals interactions, electrostatics, solvation effects, and internal strain energies, offering a more realistic estimation of the binding affinity compared to docking scores alone. The MM-GBSA results serve as a post-docking validation step, helping to rank the hit flavonoids and reference ligands based on their thermodynamic favorability. The co-crystallized ligand exhibited the most favorable binding free energy (−84.23 kcal/mol), reaffirming its optimal complementarity with the VZV-TK active site and validating the reliability of the computational protocol. This strong binding serves as an internal control, establishing an upper benchmark for ligand affinity within the evaluated chemical space. Among the screened flavonoids, Naringin dihydrochalcone displayed a notably high binding free energy (−65.14 kcal/mol), markedly outperforming both reference drugs. This result indicates a thermodynamically stable ligand–protein complex and corroborates its strong docking performance and extensive interaction network within the catalytic pocket. The favorable $\Delta G_{Binding}$ suggests efficient stabilization through cooperative electrostatic and hydrophobic contributions, consistent with the compound's multiple hydrogen bonds and deep occupancy of the binding cavity observed during interaction analysis. Myricitrin also demonstrated a favorable binding free energy (−52.66 kcal/mol), comparable to and slightly exceeding that of Famciclovir (−50.57 kcal/mol). This proximity in $\Delta G_{binding}$values suggests that Myricitrin possesses a binding efficiency similar to a clinically used antiviral, despite being a natural flavonoid scaffold. Importantly, Myricitrin's binding stability appears to arise from a balanced contribution of polar and non-polar interactions, reinforcing its potential as a viable lead compound. In contrast, Valacyclovir exhibited a substantially weaker binding free energy (−36.41 kcal/mol), reflecting limited thermodynamic stabilization at the VZV-TK active site. This observation aligns with the known pharmacological behavior of nucleoside analogs, which depend primarily on intracellular phosphorylation and subsequent inhibition of viral DNA polymerase rather than strong direct binding to thymidine kinase in its native form.

ADMET evaluation

The ADMET-relevant properties for the top-scoring compounds, alongside the controls are given in Table 4.

Table 4: Summary of druglikeness metrics from ADMET evaluation

Compound	MW	nRing	nHA	nHD	nRot	LogP	TPSA	Carcinogenicity
Naringin Dihydrochalcone	582.19	4	14	9	9	0.828	236.1	0.028
Myricitrin	464.1	4	12	8	3	1.161	210.5	0.069
Valacyclovir (Control)	324.15	2	10	5	8	-0.92	151.1	0.968
Famciclovir (Control)	321.14	2	9	2	9	0.137	122.2	0.952

In the development of potential therapeutic agents, ADMET profiling plays a critical role in predicting the pharmacokinetic behavior and safety profile of candidate molecules.[20] A compound's physicochemical properties directly influence its druglikeness, oral bioavailability, and systemic efficacy. Parameters such as molecular weight (MW), number of hydrogen bond acceptors (nHA) and donors (nHD), number of rotatable bonds (nRot), lipophilicity (logP), topological polar surface area (TPSA), and carcinogenicity prediction are routinely assessed to prioritize compounds with favorable pharmacokinetic and safety characteristics. Table 4 summarizes these ADMET-relevant properties for the top-scoring compounds, alongside the control drugs. Naringin dihydrochalcone exhibits a relatively high molecular weight (582.19 Da) and elevated polarity, as reflected by its large TPSA value (236.1 Å²). The compound possesses a substantial number of hydrogen bond donors (9) and acceptors

(14), indicating a strong capacity for polar interactions with biological targets, consistent with its favorable binding affinity toward VZV-TK. However, the high TPSA and molecular size may limit passive membrane permeability and oral bioavailability, suggesting potential challenges in systemic absorption. Despite these considerations, the moderate Log P value (0.828) indicates balanced hydrophilicity, which may mitigate solubility-related issues. Importantly, the low predicted carcinogenicity score (0.028) supports a favorable preliminary safety profile. Similarly, Myricitrin demonstrated pronounced polarity, with a TPSA of 210.5 Å², accompanied by multiple hydrogen bond donors (8) and acceptors (12). Its molecular weight (464.1 Da) is comparatively lower than that of Naringin dihydrochalcone, positioning it closer to the upper threshold of conventional druglikeness guidelines. The relatively low number of rotatable bonds (3) suggested reduced conformational flexibility, which may enhance binding specificity and reduce entropic penalties upon complex formation. A modest Log P value (1.161) further indicated acceptable aqueous solubility. The predicted carcinogenicity value (0.069) remains low, reinforcing its potential as a safe antiviral scaffold. In contrast, the reference drugs Valacyclovir and Famciclovir displayed physicochemical profiles more closely aligned with traditional small-molecule antivirals, characterized by lower molecular weights (~320 Da), reduced TPSA values (151.1 Å² and 122.2 Å², respectively), and fewer hydrogen bond donors. These features are consistent with their established oral bioavailability and clinical utility. However, both controls exhibited markedly higher predicted carcinogenicity scores (0.968 and 0.952), which, while not reflective of clinical outcomes, highlight limitations inherent to in-silico toxicity prediction models and underscore the importance of experimental validation.

Molecular Dynamic Simulation Analyses

The conformational stability and dynamic behavior of the VZV-TK protein in complex with the cocrystallized ligand, myricitrin, and naringin dihydrochalcone were systematically investigated using complementary molecular dynamics (MD) descriptors, including root mean square deviation (RMSD), root mean square fluctuation (RMSF), intermolecular hydrogen bond occupancy, radius of gyration (Rg), and solvent accessible surface area (SASA). Collectively, these metrics provide a comprehensive view of both global structural integrity and local binding-site dynamics, enabling reliable discrimination among ligand candidates based on their dynamic performance. RMSD analysis was employed to evaluate the conformational stability of the VZV-TK protein in complex with the cocrystallized ligand, myricitrin, and naringin dihydrochalcone over the molecular dynamics simulation (Figure 4). RMSD values below ~2.0 Å are generally indicative of highly stable protein–ligand complexes, whereas sustained deviations above ~3.0 Å may suggest increased structural flexibility or reduced binding persistence.[21] RMSD analysis revealed rapid equilibration and sustained stability for the reference VZV-TK–cocrystallized ligand complex, which converged within the first 5–10 ns and stabilized in the range of ~1.6–1.9 Å. This narrow plateau, maintained throughout the simulation, reflects preservation of the native protein fold and persistent ligand anchoring within the active site. The VZV-TK–myricitrin complex exhibited an equally rapid equilibration profile but stabilized at an even more tightly confined RMSD range of ~1.7–1.8 Å, with minimal temporal fluctuations (<±0.15 Å). Such low and consistent deviations are indicative of an exceptionally stable binding mode, suggesting that myricitrin integrates optimally into the active-site architecture without inducing unfavorable backbone rearrangements. In contrast, the VZV-TK–naringin dihydrochalcone complex displayed substantially higher RMSD values, fluctuating between ~2.0 and 2.2 Å, with occasional excursions approaching ~2.8 Å, indicative of increased conformational plasticity and less persistent ligand accommodation. These global stability trends are further substantiated by residue-level RMSF analysis (Figure 5).

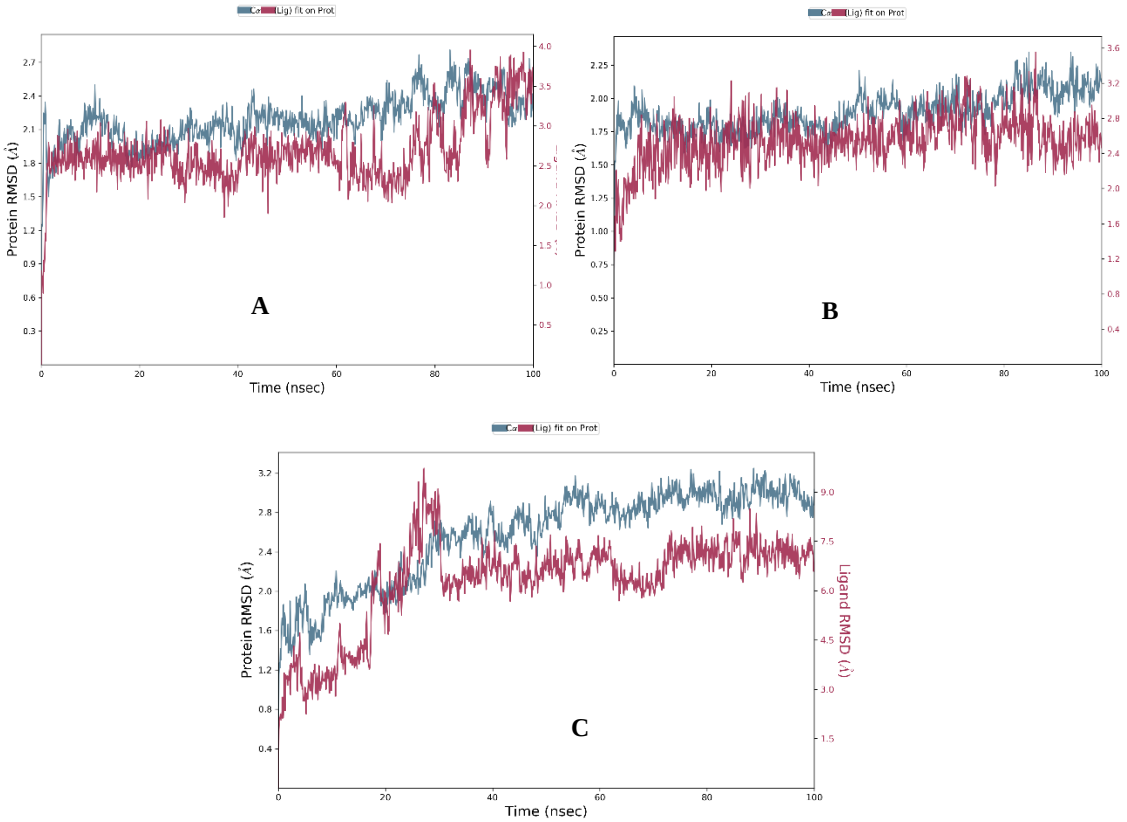

Figure 4: Root Mean Square Deviation of (A) VZV-TK – Cocrystallized Ligand (B) VZV-TK – Myricitrin (C) VZV-TK – Naringin dihydrochalcone complexes

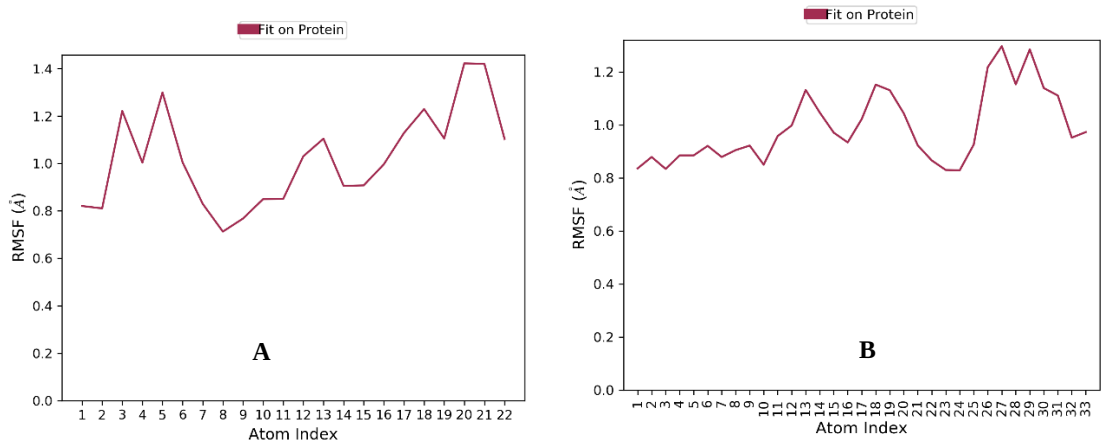

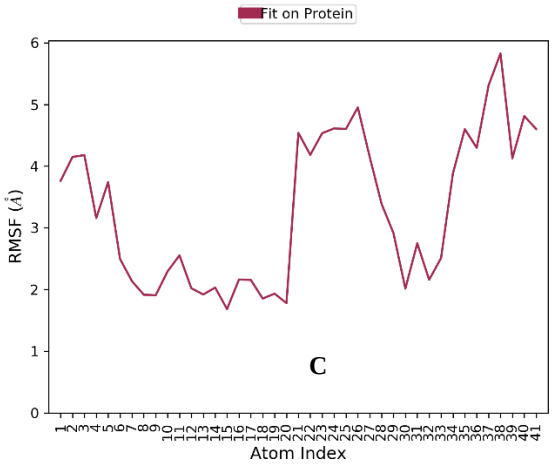

Figure 5: Root Mean Square Fluctuation per residue of (A) VZV-TK – Cocrystallized Ligand (B) VZV-TK – Myricitrin (C) VZV-TK – Naringin dihydrochalcone complexes

In both the cocrystallized ligand and myricitrin complexes, the majority of protein residues, particularly those forming the catalytic core and binding pocket exhibited restrained fluctuations, generally remaining below ~1.4 Å. Notably, active-site residues in the myricitrin-bound system showed reduced flexibility compared to the reference complex, suggesting enhanced local stabilization mediated by persistent ligand interactions. Conversely, the naringin dihydrochalcone complex demonstrated elevated RMSF values in loop regions adjacent to the binding site, with fluctuations reaching ~5.5 Å. These localized increases in flexibility likely contribute to the higher RMSD observed for this complex and reflect a less rigid binding environment.

Intermolecular hydrogen bond analysis provides mechanistic insight into the stability differences observed among the complexes (Figure 6).

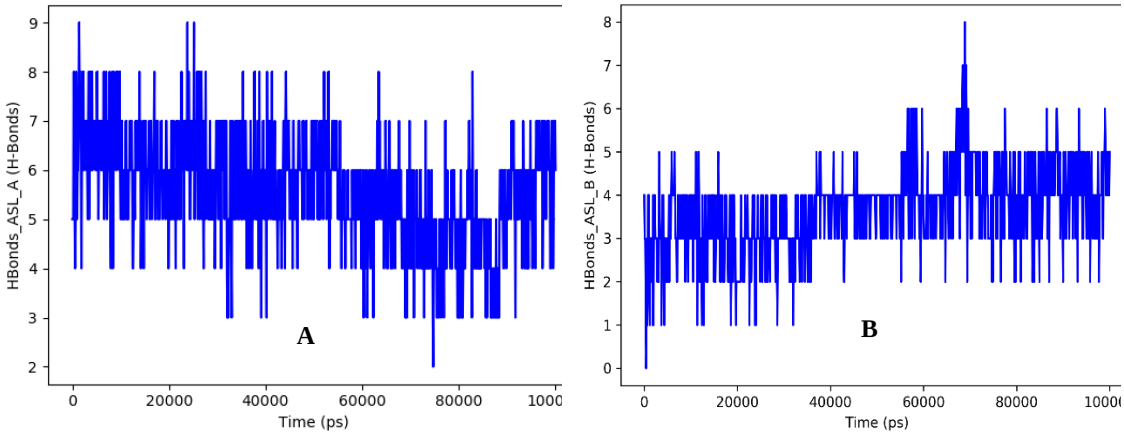

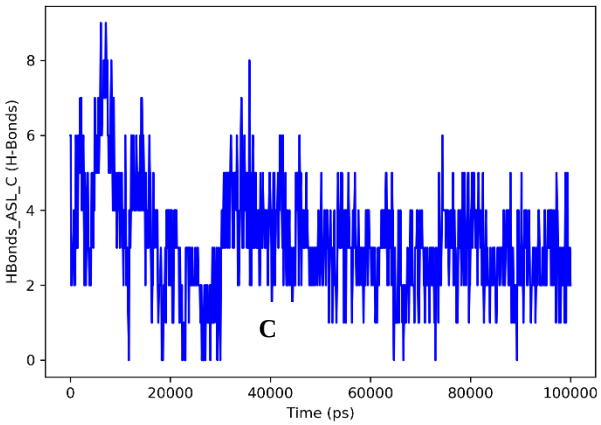

Figure 6: Intermolecular Hydrogen Bonds formed between (A) VZV-TK – Cocrystallized Ligand (B) VZV-TK – Myricitrin (C) VZV-TK – Naringin dihydrochalcone complexes

The VZV-TK–cocrystallized ligand complex exhibited a stable hydrogen-bonding pattern, with the dominant population centered between 5-7 hydrogen bonds, indicating a consistent interaction network that supports the native binding mode. Similarly, the VZV-TK–myricitrin complex maintained a persistent 3–5 hydrogen bond network throughout most of the simulation, reflecting effective polar complementarity with key active-site residues. The multiple hydroxyl groups of myricitrin enable sustained donor–acceptor interactions, contributing to reduced ligand mobility and the low RMSD (~1.7–1.8 Å) observed for this complex. The VZV-TK–naringin dihydrochalcone complex however displayed a less stable hydrogen-bonding profile, with the densest population shifting toward 2–4 hydrogen bonds after equilibration. The lower hydrogen-bond occupancy and frequent formation–breakage events are indicative of weaker interaction persistence and greater conformational flexibility, consistent with its higher RMSD and increased residue-level fluctuations. The hydrogen-bond analysis supports the superior dynamic stability of the myricitrin-bound complex relative to naringin dihydrochalcone and reinforces its classification as the most promising ligand among those evaluated. Analyses of global protein compactness further reinforce these findings. The radius of gyration (Rg) for both the cocrystallized ligand and myricitrin complexes remained stable at ~20.0–20.2 Å, with minimal fluctuations, indicating maintenance of a compact and well-folded protein structure throughout the simulation (Figure 7).

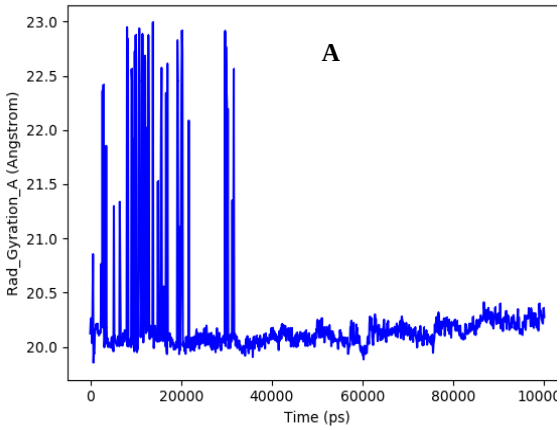

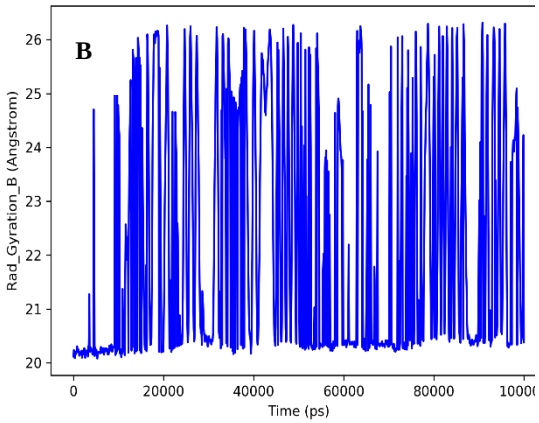

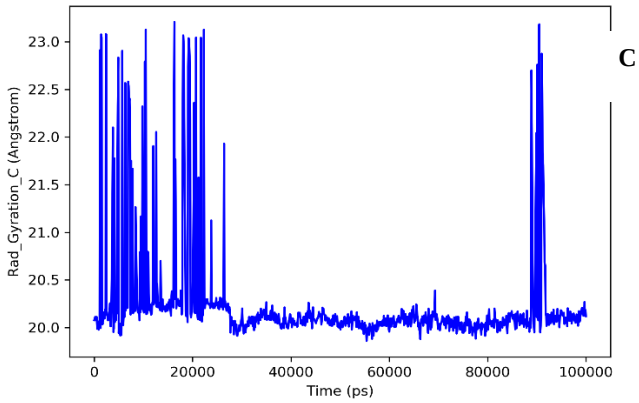

Figure 7: Radius of Gyration of (A) VZV-TK – Cocrystallized Ligand (B) VZV-TK – Myricitrin (C) VZV-TK – Naringin dihydrochalcone complexes

Similarly, SASA values for the cocrystallized ligand and myricitrin complexes were tightly clustered in the range of ~14,700–15,300 Å2 and 14,800–15,200 Å2 respectively, suggesting limited solvent exposure and preservation of the protein's tertiary architecture (Figure 8).In contrast, the naringin dihydrochalcone complex exhibited higher and more variable Rg (~20.0–20.4 Å) and SASA (~14,300–15,300 Å2) values, indicative of transient structural expansion and increased solvent accessibility, further supporting reduced global stability.

The strong concordance across all MD descriptors highlights myricitrin as the most dynamically favorable ligand among those evaluated. Its ability to stabilize the VZV-TK protein at a consistently low RMSD, suppress residue-level fluctuations within the active site, maintain a robust hydrogen-bonding network, and preserve global protein compactness underscores its superior binding stability relative to naringin dihydrochalcone. The close similarity between the myricitrin and cocrystallized ligand complexes further suggested that myricitrin effectively mimics the stabilizing interactions of the native ligand, reinforcing its potential as a promising flavonoid-based inhibitor of the VZV-TKprotein.

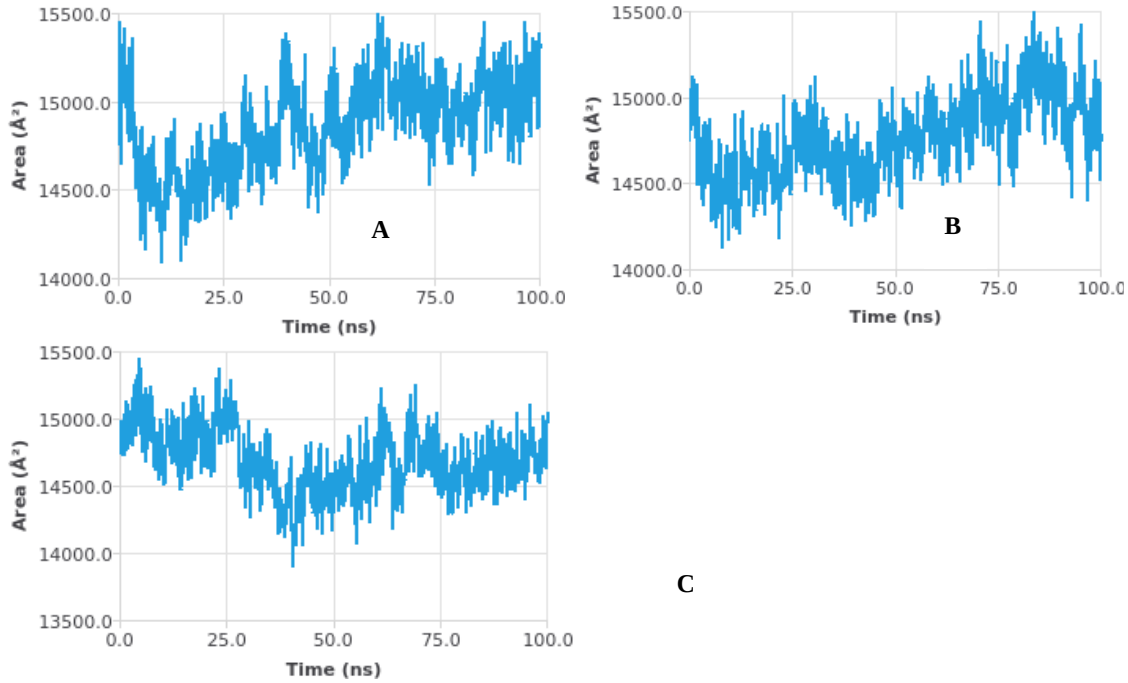

Figure 8: Solvent Accessible Surface Area of (A) VZV-TK – Cocrystallized Ligand (B) VZV-TK – Myricitrin (C) VZV-TK – Naringin dihydrochalcone complexes

CONCLUSION

This study employed an integrated structure-guided in-silico approach to identify flavonoid-based inhibitors of Varicella-Zoster Virus thymidine kinase (VZV-TK). Molecular docking and MM-GBSA analyses revealed that neohesperidin dihydrochalcone, naringin dihydrochalcone, and myricitrin exhibit strong binding affinities and favorable thermodynamic stability compared with clinically used antivirals. Molecular dynamics simulations further highlighted myricitrin as the most dynamically stable ligand, demonstrating persistent hydrogen bonding, low conformational deviation, and preserved protein compactness comparable to the co-crystallized reference ligand. ADMET profiling indicated acceptable physicochemical properties and low predicted toxicity for the top candidates. These findings support flavonoid scaffolds as promising leads for VZV inhibition and provide a robust computational foundation for subsequent in-vitro and in-vivo validation toward the development of safer antiviral therapeutics.

CONFLICT OF INTEREST

The authors declare no conflict of interest.

AUTHORS DECLARATION

The authors hereby declare that the works presented in this article are original and that any liability for claims relating to the content of this article will be borne by them.

REFERENCES

1. Tommasi C, Breuer J. The Biology of Varicella-Zoster Virus Replication in the Skin. Viruses. 2022;14(5):982.
2. Shah HA, Meiwald A, Perera C, Casabona G, Richmond P, Jamet N. Global Prevalence of Varicella-Associated Complications: A Systematic Review and Meta-Analysis. Infectious Diseases and Therapy. 2023;13(1):79–103.
3. Grose C. Surveillance of Nigerian children suggests that varicella may be a risk factor for acquisition of monkeypox. Frontiers in Public Health. 2023;11.
4. Ishihara R, Watanabe R, Shiomi M, Katsushima M, Fukumoto K, Yamada S, Okano T, Hashimoto M. Exploring the Link between Varicella-Zoster Virus, Autoimmune Diseases, and the Role of Recombinant Zoster Vaccine. Biomolecules. 2024;14(7):739.
5. Papaevangelou V, Quinlivan M, Lockwood J, Papaloukas O, Sideri G, Critselis E, Papassotiriou I, Papadatos J, Breuer J. Subclinical Varicella-Zoster Virus reactivation in immunocompetent children hospitalized in the ICU associated with prolonged fever duration. Clinical Microbiology and Infection.2013;19(5):E245–E251.
6. Tayyar R, HoD. Herpes Simplex Virus and Varicella Zoster Virus Infections in Cancer Patients. Viruses. 2023;15(2):439.
7. AhmadF, SachdevaA, SahB. K, Kumar A, Kumar R, Seksaria B. A review of herbal therapeutics for the prevention and management of poxvirus infections. Archives of Microbiology.2025;207(8).
8. Sharma S, Ghosh P, Kar C, Ghosh R. Anticipating Viral Challenges: A Perspective on Phytochemicals against Existing and Emerging Viruses. Anti-Infective Agents. 2025;23(3).
9. Outbreak of chickenpox at Benue's IDP camp. Daily Post Nigeria. (2023, August 28). Available from: https://dailypost.ng/2023/08/28/outbreak-of-chickenpox-at-benues-idp-camp/
10. Olumade T. J, Adesanya O. A, Fred-Akintunwa IJ, Babalola DO, Oguzie JU, Ogunsanya OA, George UE, Akin-Ajani OD, Osasona DG. Infectious disease outbreak preparedness and response in Nigeria: history, limitations and recommendations for global health policy

and practice. AIMS Public Health. 2020;7(4):736–757.

11. Omoboyowa DA, Kareem JA, Saibu OA, Bodun DS, Ajayi TM, Oyeneyin OE. Identification of phyto-compounds from Ilex kudingcha as inhibitors of sterol-14α demethylase protease: A computational approach against Chagas disease. Chemistry Africa.2022;6(3):1335–1347.
12. Bodun DS, Omoboyowa DA, Omotuyi OI, Olabisi AO, Oyinloye BE, Abioye AE, Adegboyega AE, Akindele OO, Irekeola AA, Agunu A. QSAR-based virtual screening of traditional Chinese medicine for the identification of mitotic kinesin Eg5 inhibitors. Computational Biology and Chemistry.2023;104: 107865.
13. Duru CE, and Chidiebere CW. Computer-assisted discovery of tyrosinase inhibitors from turmeric and clove: an in silico study on natural skin whitening agents and their potential toxicity. South African Journal of Botany. 2024;175:669-683.
14. Nwofor OK, Duru CE, Nwofor CN. In-vitro, bioinformatics, and computational biophysical analyses of antifungal phytochemicals from Acalypha wilkisiana variants targeting Malassezia lipase. Trop J Drug Res. 2025;2(9):231–244.
15. Chidiebere CW, Duru CE, Mbagwu JPC. Application of computational chemistry in chemical reactivity: A review. J Niger Soc Phys Sci. 2021; 3:292–297.
16. Ikezu UM, Duru CE, Ikpa CB, Ibe FC. In silico discovery of dual-targeting molecules from Acalypha wilkesiana against hypertension and hyperglycemia. Discover Chemistry. 2025;2(1).
17. Durrant JD, McCammon JA. Molecular dynamics simulations and drug discovery. BMC Biology. 2011;9(1):71.
18. Hou T, Wang J, Li Y, Wang W. Assessing the performance of the MM/PBSA and MM/GBSA methods:II. The accuracy of binding free energy calculations based on molecular dynamics simulations. Journal of Chemical Information and Modeling. 2010;32(5):866–877.
19. Forouzesh N, Mishra N. An effective MM/GBSA protocol for absolute binding free energy calculations: A case study on SARS-CoV-2 spike protein and the human ACE2 receptor. Molecules. 2021;26(8):2383.
20. Duru IA, Enenebeaku UE, Ngozi-Olehi LC, Enyoh CE, Duru CE, Umar HI, Kuthi NA, Kurma N, Dharmarpu V. Experimental and computational insights into Gangronema latifolium leaf compounds as GLP-1 receptor agonists. Chemistry Africa. 2024;7(5), 2581–2597.
21. Duru CE, Izuagba FO, Duru IA, Nwakile TI, Nwadike CD. Computational structure-based identification of silymarin as a promising flavonoid inhibitor of the diphtheria toxin catalytic domain. Discover Chem. 2025;2:286.